J Mater Sci: Mater Med (2016) 27:105
DOI 10.1007/s10856-016-5716-3

BIOMATERIALS SYNTHESIS AND CHARACTERIZATION

Original Research

Effects of hydroxyapatite/Zr and bioglass/Zr coatings on morphology and corrosion behaviour of Rex-734 alloy

Y. Say[1] · B. Aksakal[2]

Received: 11 February 2016 / Accepted: 9 April 2016 / Published online: 19 April 2016

Abstract To improve corrosion resistance of metallic implant surfaces, Rex-734 alloy was coated with two different bio-ceramics; single-Hydroxyapatite (HA), double-HA/Zirconia(Zr) and double-Bioglass (BG)/Zr by using sol–gel method. Porous surface morphologies at low crack density were obtained after coating and sintering processes. Corrosion characteristics of coatings were determined by Open circuit potential and Potentiodynamic polarization measurements during corrosion tests. Hardness and adhesion strength of coating layers were measured and their surface morphologies before and after corrosion were characterized by scanning electron microscope (SEM), XRD and EDX. Through the SEM analysis, it was observed that corrosion caused degradation and sphere-like formations appeared with dimples on the coated surfaces. The coated substrates that exhibit high crack density, the corrosion was more effective by disturbing and transmitting through the coating layer, produced CrO_3 and Cr_3O_8 oxide formation. It was found that the addition of Zr provided an increase in adhesion strength and corrosion resistance of the coatings. However, BG/Zr coatings had lower adhesion strength than the HA/Zr coatings, but showed higher corrosion resistance.

✉ B. Aksakal
baksakal2@gmail.com

Y. Say
yakupsay1@gmail.com

[1] Department of Metallurgical and Materials Engineering, Engineering Faculty, Tunceli University, 62000 Tunceli, Turkey

[2] Department of Metallurgical and Materials Engineering, Faculty of Chemical and Metallurgical and Materials Engineering, Yıldız Technical University, 34220 Istanbul, Turkey

1 Introduction

Biomaterials used in different fields such as medicine, dentistry, veterinary, and pharmacy should have adequate mechanical strength and corrosion resistance along with high biocompatibility. These characteristics are generally provided with metallic biomaterials, e.g. stainless steels widely used in especially orthopedic applications due to low cost and superior mechanical properties [1–3]. Even though metallic biomaterials have adequate strength characteristics, they remain incapable in terms of corrosion resistance in life body environment. This incapability causes corrosion and consequently implant loosening and free metal ion release such as Fe, Ni, and Cr [4, 5]. For this reason, the studies on improving the bioactivity, biocompatibility, and corrosion resistance of metallic biomaterials are world wide studied continued [6–11]. Previous studies reported that hydroxyapatite (HA) enhanced the biocompatibility characteristics of metallic implants and increased the corrosion resistance of coating applications due to its bone-like structure and superior biocompatibility characteristics. Due to perfect biocompatibility and bioactivity, HA is preferred in coating applications on metallic surfaces. Therefore, it is recommended to coat metallic implants with HA in order to increase biocompatibility and corrosion resistance [7, 12–17].

Furthermore, HA, which is a biodegradable or absorbable biocompatible material, is capable of forming strong chemical bonds with natural bone tissue due to its characteristic properties [18]. Along with its biocompatibility characteristics, bone-like structure of HA was determined to increase bone formation in implant applications [19, 20]. As well as HA, Bioglass (BG) is also used as surface coating material in order to improve bioactivity,

biocompatibility and corrosion resistance of metallic materials [11, 21–23].

Various additions such as TiO_2 [24], Y_2O_3–Zr are made in order to improve biocompatibility, corrosion and adhesion properties of HA and BG used in surface coatings performed on metallic biomaterials [9–11, 24]. It was reported that the addition of Al_2O_3 and ZrO_2 in certain amounts improved mechanical properties and addition of ZrO_2 also increased toughness in HA and 45S5 bioactive glass [25, 26].

In order to functionalize metallic implants, Rex-734 alloy was single HA-BG and double HA-BG/Zr dip coated. The effects of addition of Zr into HA and BG on surface morphology, hardness, adhesion, and corrosion strength were comparatively examined in this study.

2 Materials and methods

2.1 Materials

As substrate material, 8-mm diameter cylindrical Rex-734 (ASTM F1586 Hard–HI, Sandwick) samples, whose chemical composition was shown in Table 1, were used. Substrates were cut into 10×20 mm^2 small samples for characterization examinations and 60×8 mm^2 large samples (width and length) for shearing tests. Samples were machined sensitively performed with 1-mm SiC cutting discs. Sand blasted process with SiO_2 particles in particle size of 90 microns at 6 bar pressure was applied onto surfaces of the prepared metallic samples before surface coating. Then they were subjected to ultrasonic cleaning process in distilled water, acetone and HNO_3.

2.2 Coating

Three types (Groups: G1, G2 and G3) of coatings as Single-HA (G1), HA/Zr (G2), and BG/Zr (G3), were applied on Rex-734 alloy substrates by using the sol–gel method. HA and BG (45S5) based sols were prepared for HA and BG based coatings performed and to ease gelation and sinterability P_2O_5, $NaCO_3$ and KH_2PO_4, were added, respectively. The prepared sol was ultrasonically homogenized until a homogenous gel was obtained using the compositions given in Table 2. The obtained gel samples were dired and characterized. The substrates were coated at an immersion rate of 10 mm/s. Coated samples were kept under room conditions and then they were subjected to the pre-drying in the furnace and later subjected to sintering process at 750 °C.

Table 1 Chemical composition of REX-734 alloy (Sandwick)

Elements (wt%)									
C	Cr	Cu	Mn	Mo	N	Nb	Ni	Si	Fe
0.031	20.68	0.13	4.12	2.27	0.38	0.28	9.59	0.47	62.05

Table 2 Sol–gel concentrations (determined during sol–gel processes)

Coating groups	Coating substitutes (mol %)					
	HA	BG	P_2O_5	KH_2PO_4	$NaCO_3$	Zr
Uncoated (G0)	–	–	–	–	–	–
HA (G1)	40	–	30	10	20	–
HA/Zr (G2)	40	–	20	10	20	10
BG/Zr (G3)	–	40	20	10	20	10

2.3 Mechanical tests

Adhesion strength of the coatings achieved on the substrates was measured by using shearing test. DP460 epoxy (3 M) was used as adhesive in tests. Adhesion sample pairs, one of which was coated and the other one was uncoated, were reciprocally adhered with surface areas having a 15-mm length and an 8-mm width. The tests were carried out via tensile test (Shimadzu AG-X) having a 50 kN capacity, in accordance with ASTM C 633 standards at the tensile rate of 2 mm/min. Mean adhesion values were determined by performing three tests for each sample group. Hardness measurements of the coatings were performed with pyramidal Vickers indenter (136°) (0.098 − 98 N/0.01 − 10 kgf) hardness test machine (Emco test, Durascan) and mean values were calculated by performing six samples for each group.

2.4 Corrosion

The corrosion tests were performed in order to examine the effect of the coatings on corrosion resistance of metallic substrate. Corrosion samples were taken into cold bakelite in such a way that only the coated surfaces were left as uncovered by bakelite. Before the samples were taken into bakelite, in order to ensure conductivity the uncoated surface of substrates were fixed with copper wires with a 1.7 mm diameter for corrosion tests and the conductivity controls were carried out. The tests were performed in Ringer solution medium (37 °C) corrosion test unit Gamry PCI14/750 (USA) by using three-electrode technique. In the tests, saturated silver/silver chloride electrode (Ag/AgCl) was used as the reference electrode (RE), platinum wire (Pt) was used as the contrary electrode (CE) and the corrosion samples were also used as the working electrode (WE). Repeatability was determined by performing at least two tests for each sample group. Open circuit potential measurements (OCP) and potentiodynamic polarization

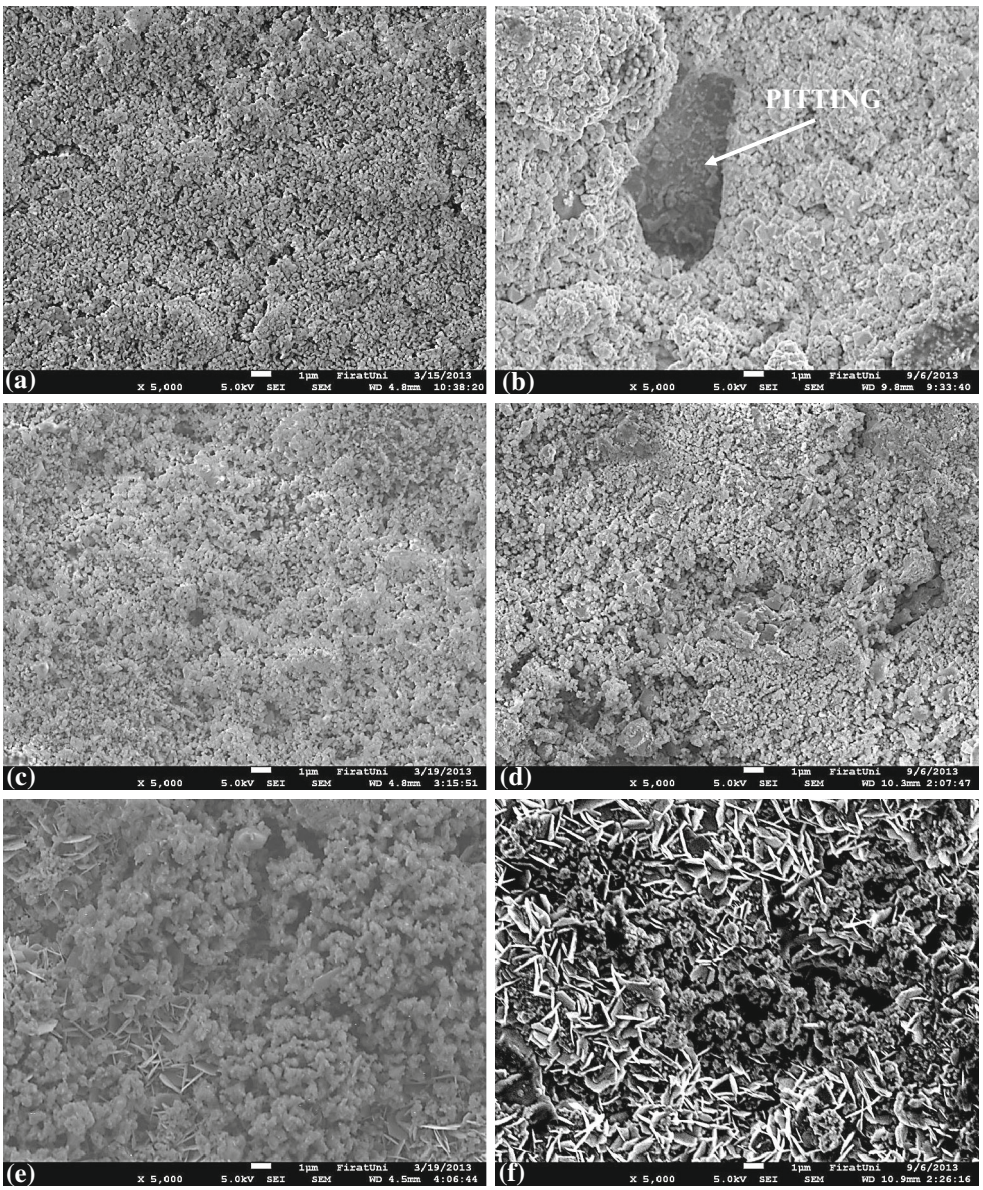

Fig. 1 SEM views before corrosion: **a** HA, **c** HA/Zr, **e** BG/Zr and after corrosion: **b** HA, **d** HA/Zr, **f** BG/Zr

measurements (PDS) were carried out at the scanning rates of 1 mV/s. It was tried to determine localized interactions of the samples by specifying time dependent variation (dE-t) of the mixed potential. In addition, their polarization curves and corrosion characteristics were also determined.

2.5 Surface analysis

The surface morphologies of the coatings were examined by using scanning electron microscope, SEM (JEOL JSM 7001F) at different magnifications. Analysis spectra of displayed regions (EDX) were detected by using Oxford INCA System X-ray spectrometer. For XRD analyses, XRD device (Bruker D8 Advance) with a Kα tube was used and the analyses were performed with a pitch rate of 0.02 between 10° and 90° at a wavelength of 1.5406 (λ). Film thickness of the coatings was determined by using computer assisted Nikon Eclipse MA200 optical microscope with a magnification of ×1000. Measurements of coating thickness from different regions were performed by using optical images and mean coating thickness values were then determined.

3 Results

Film thickness values of averagely 11 μm were obtained from HA, HA/Zr, and BG/Zr coatings applied to the surface of Rex-734 alloy. Hardness measurements taken from

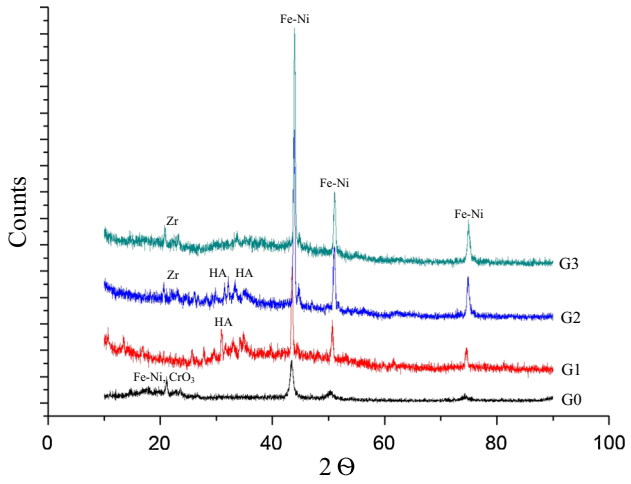

Fig. 2 XRD spectrums before corrosion

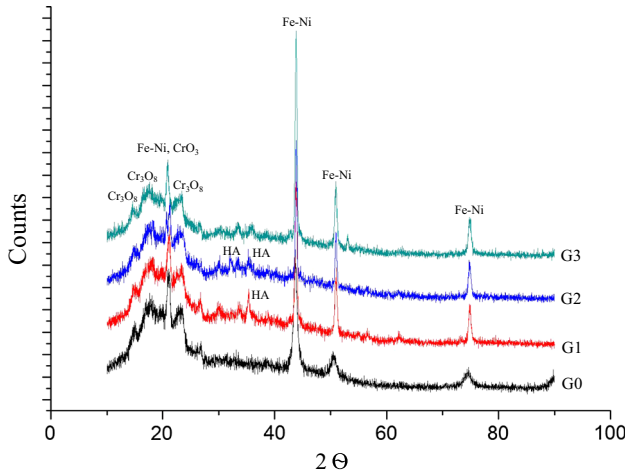

Fig. 3 XRD spectrums after corrosion

surface coatings revealed that while the surface hardness was 290.2 HV in HA coatings, it increased to 353.2 HV with the addition of Zr into HA. Hardness in coatings with addition of Zr into BG was measured as 137.1 HV. While adhesion strength in HA coatings applied to surface of Rex-734 was 25.14 MPa, adhesion strength in HA/Zr coatings increased and adhesion strength was measured as 27.04 MPa. Adhesion strength in BG/Zr coatings was measured as 13.45 MPa.

SEM analyses showed that the coatings exhibit porous surface morphologies at low crack density (Fig. 1a, c, e). It was observed that the corrosion caused destruction in agglomerated, sphere-like structure of the coating and led to formation of dimples in the surface (Fig. 1b, d, f). XRD analyses indicated that the corrosion reached to the substrate by passing over coating and caused formation of CrO_3–Cr_3O_8 oxides (Figs. 2, 3). The damage caused by the corrosion in the coating appeared as a decrease at the Ca/P ratios and an increase at the O, Fe, Ni and Cr ratios (Figs. 4, 5).

Figure 6 shows OCP changes of uncoated Rex-734 and the coated samples in the Ringer Solution. Figure 7 shows comparatively PDS of the samples. Table 3 shows some corrosion parameters calculated from OCP and PDS curves.

4 Discussion

HA and BG having high biocompatibility was used for the coatings applied in order to improve biocompatibility, osteointegration, and corrosion characteristics of metallic implant, Rex-734 surfaces. Porous coating surface morphology having a low crack density is desired in order to enhance osteointegration in the coatings. SEM examinations indicated that surface morphology having a low crack density was achieved in all coatings before corrosion (Fig. 1a, c, e).

Another issue required in the surface coatings is adhesion strength of the coating. The coatings applied with metallic biomaterials are required to have adhesion strength at a level in which will not separate from surface during implantation. In group G1, the adhesion strength of 25.14 MPa was obtained. An approximately 8 % increase (up to 27.04 MPa) was detected in the adhesion strength with addition of 10 % Zr into HA. It was thought that thermal expansion difference between metallic implants and the materials used in surface coatings caused crack formation during drying and sintering processes. These cracks observed in the surface coatings affected negatively adhesion strength of coatings. The main goal in addition of Zr into HA is to obtain or minimize cracks on coating surfaces and increasing fracture toughness and adhesion strength. Similar aims were also reported with addition of Yttria/ZrO_2 into HA coatings [10]. Hardness measurement results of the coatings had proportionality with adhesion strengths. Addition of Zr into HA provided an increase for both hardness and adhesion strength of the coatings. However, BG/Zr coatings showed quite low hardness results and adhesion strength compared to HA/Zr coatings.

It was observed that sphere-like structure of the coatings and dimples were formed on the surface (Fig. 1b, d, f). EDX analyses indicated that a Ca-P-O based structure dominated the surface in only HA coated samples (Fig. 4). However, a decrease occurred in Ca/P ratio and an increase occurred in Fe–Ni ratio from substrate as a result of corrosion (Fig. 5). Such results suggest that the corrosion reached to the metallic substrate by transmitting through the minimal cracks in coated substrates. XRD analysis showed that the formation of CrO_3 and Cr_3O_8 oxides on surface of sample G1 after corrosion also supports the

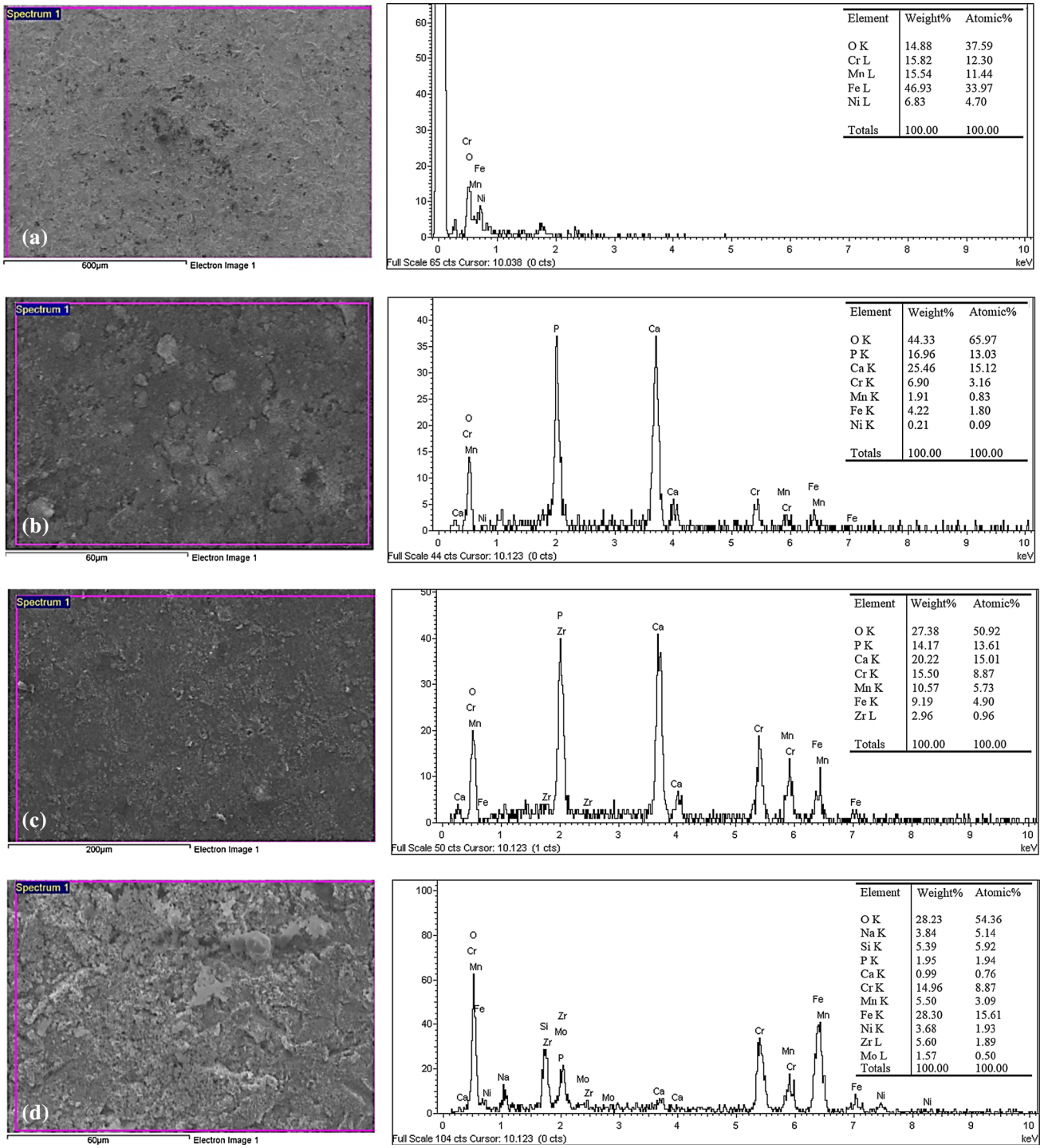

Fig. 4 SEM micrographs and EDX picture before corrosion **a** uncoated (G0), **b** HA coated (G1), **c** HA/Zr coated (G2) and **d** BG/Zr coated (G3) samples

current results (Figs. 2, 3). Differently from samples in G1, no decrease was observed in Ca/P ratio in samples G2 after corrosion process. However, XRD analyses showed the presence of CrO_3 and Cr_3O_8 oxide formation also in G2 group samples after corrosion (Fig. 3). While EDX analysis of BG/Zr coatings before corrosion shows the existence of BG, consisting of Si–Ca–Na–P–O compound the presence of Zr used as additive. From Fe–Cr–Ni content, Cr was detected belonging to the substrate of Rex-734. Additionally, it was observed that the content of

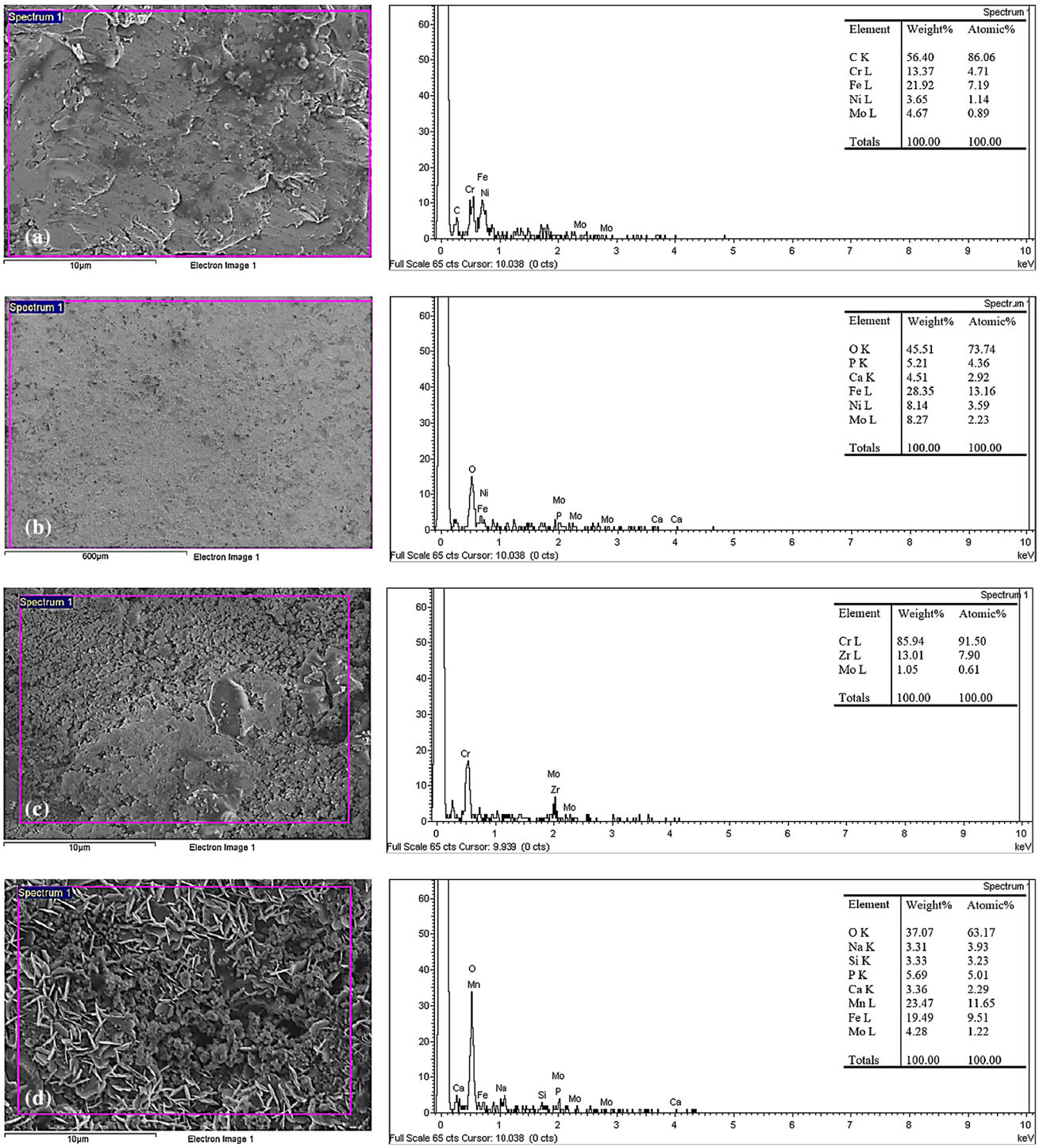

Fig. 5 SEM micrographs and EDX picture after corrosion **a** uncoated (G0), **b** HA coated (G1), **c** HA/Zr coated (G2) and **d** BG/Zr coated (G3) samples

coating (Si–Ca–Na–P) was significantly decreased and peaks of Fe–Mn–Mo from substrate appeared in EDX analysis after corrosion. This result indicated that the corrosion caused a considerable deformation in the coating and reached to the substrate by passing over coating in G3 group samples.

Figure 6 shows changes of OCP in Ringer solution under in vitro conditions. While E_{ocp} in uncoated sample G0 increased depending on time, E_{ocp} value decreased depending on time in all the coated samples. It was observed that the coated samples became stabilized in a shorter time with Ringer's solution and had lower potential

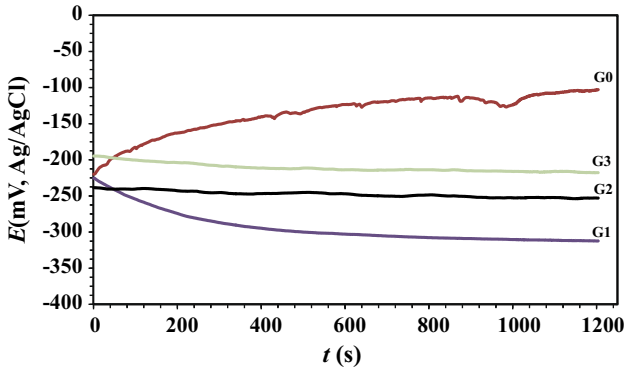

Fig. 6 Results of OCP analysis; uncoated (G0), HA coated (G1), HA/Zr coated (G2) and BG/Zr coated (G3) samples

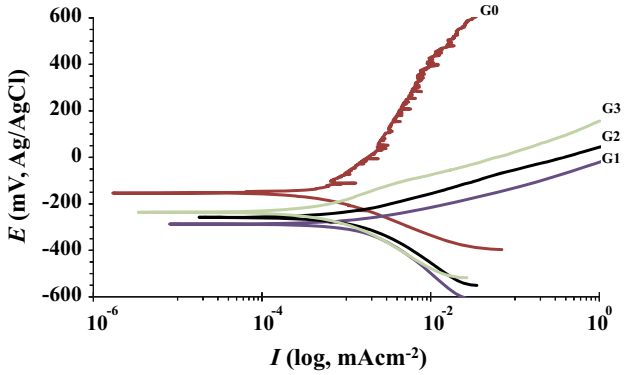

Fig. 7 Results of PDS analysis; uncoated (G0), HA coated (G1), HA/Zr coated (G2) and BG/Zr coated (G3) samples

vibration amplitudes compared to uncoated samples. The samples G2 and G3 became stabilized in a shorter time compared to sample G1. The change in the E_{ocp} values of the coatings towards more anodic potentials depending on the time in the Ringer solution compared to the initial potentials showed the presence of localized corrosion on the surface.

Figure 7 shows comparatively PDS of coated and uncoated samples in Ringer solution and at body temperature (37 °C). The samples were over polarized in the anodic direction by increasing potential in order to reveal differences of corrosion. Curves obtained as a result of PDS analysis show that the potential in the cathodic region increased in all the samples and the current regularly decreased. This situation indicated that the corrosion occurred as an activation-controlled corrosion mechanism. I_{corr}, which was 1.03 μA in sample G0, increased to 1.65 μA 1. This increase in I_{corr} value pointed out that the HA coating increased the corrosion rate of Rex-734 substrate. However, the values at nA level signified that there was no significant difference. Additionally, the decrease in the anodic slope (β_A) from 562.2×10^{-3} V/dec. to 88×10^{-3} V/dec. in the HA coated surface showed that the anodic activities decreased on the surface. Consequently, it was observed that single-HA coating did not provide the increase expected for corrosion resistance. Similar results were also reported in the HA coatings containing Y_2O_3–Zr applied on 316 L substrates [18] and in the HA-Nb coatings applied by using the plasma spray [19, 27]. The fact that the expected increase in corrosion resistance was not observed associated with the porous structure of the coating (Fig. 1a).

It was thought that the porous HA coating, the morphology negatively affected the corrosion protection and also caused localized corrosion on the coated sample surface. These pores were the zones where electrolyte (Ringer solution) was still and in time, the internal parts of these porosities covered with oxide-structured corrosion products. If the Cl^- ions increase in this zone compared to the other zones of the surface, such zones may become the localized areas where surface conductivity and the dissolution of oxide film to increase. In other words, this is an indication that these porosities can also act as the preferred corrosion zones. It was observed that the addition of Zr into HA caused a decrease in corrosion rate and increased the polarization resistance (Table 3). This situation can be explained as the fact that the addition of Zr slowed down the corrosive products to reach the metallic substrate by covering pores of HA and the products to peeled off from the surface. When BG coatings were compared with HA and HA/Zr coatings, it could be asserted that the BG-based coatings found more stable surface protection compared to the HA coated ones. Although the base material was the same in all samples, the fact that I_{corr} values showed differences in a wide range for all samples and revealed that the corrosion rate was variable for each sample.

Table 3 Corrosion parameters of the sample groups determined through the Taffel curves

Coating groups		Eocp (mV)	Ecorr (mV)	Icorr ($\times 10^{-9}$ A/cm^2)	β_A ($\times 10^{-3}$ V/dec.)	β_C ($\times 10^{-3}$ V/dec.)
G0	Uncoated (control)	−97	−153	1030	562.2	187.5
G1	HA	−313	−287	1650	88	263
G2	HA/Zr	−251	−258	1220	116	205
G3	BG/Zr	−217	−236	655	185	181

5 Conclusions

A porous surface morphology in a sphere-like form with low crack densities were obtained in Single-HA, double-HA/Zr and double BG/Zr coatings. It was determined that BG coatings showed lower hardness and adhesion strength values than HA coatings and addition of Zr into HA increased hardness and adhesion strength. When the coatings were exposed to corrosion, it was observed that sphere-like grain structures and dimples were formed. It was found that corrosion resistance did not increase due to localized corrosion in the Single-HA coatings, however, the addition of Zr into HA increased the corrosion resistance as well as adhesion strength. It was observed that BG coatings produced more stable surface protection and better corrosion resistance compared to HA and HA/Zr coatings.

References

1. Singh V, Marchev K, Cooper CV, Meletis EI. Intensified plasma-assisted nitriding of AISI 316L stainless steel. Surf Coat Technol. 2002;160:249–58.
2. Ratner BD, Hoffman AS, Schoen FJ, Lemons JE. Biomaterial science: an introduction to material in medicine. San Diego: Academic Press; 1996.
3. Sumita M. Present status and future trend of metallic materials used in orthopedics. Orthop. Surg. 1997;48:927–34.
4. Placko HE, Brown SA, Payer JH. Release of cobalt and nickel from a new total finger joint prosthesis made of vitallium. J Biomed Mater Res. 1983;17:655–68.
5. Tiwari SK, Mishra T, Gunjan MK, Bhattacharyya AS, Singh TB, Singh R. Development and characterization of sol–gel silica–alumina composite coatings on AISI 316L for implant applications. Surf Coat Technol. 2007;201:7582–8.
6. Liu DM, Yang Q, Troczynski T. Sol–gel hydroxyapatite coatings on stainless steel substrates. Biomaterials. 2002;23:691–8.
7. Balamurugan A, Balossier G, Kannan S, Rajeswari S. Elaboration of sol-gel derived apatite films on surgical grade stainless steel for biomedical applications. Mater Lett. 2006;60:2288–93.
8. Fathi MH, Mohammadi AD. Preparation and characterization of sol–gel bioactive glass coating for improvement of biocompatibility of human body implant. Mater Sci Eng A. 2008;474:128–33.
9. Salehi S, Fathi MH. Fabrication and characterization of sol-gel derived Hydroxyapatite/Zirconia composite nanopowders with various Yttria contents. Ceram Int. 2010;36:1659–67.
10. Balamurugan A, Balossier G, Kannan S, Michel J, Faure J, Rajeswari S. Electrochemical and structural characterisation of zirconia reinforced hydroxyapatite bioceramic sol–gel coatings on surgical grade 316L SS for biomedical applications. Ceram Int. 2007;33:605–14.
11. Garcia C, Cere S, Duran A. Bioactive coatings prepared by sol–gel on stainless steel 316L. J Non-Cryst Solids. 2004;348:218–24.
12. Kannan S, Balamurugan A, Rajeswari S. H_2SO_4 as a passivating medium on the localised corrosion resistance of surgical 316L SS metallic implant and its effect on hydroxyapatite coatings. Electrochim Acta. 2004;49:2395–403.
13. Aksakal B, Dikici B, Sonmez S. Corrosion protection of AA6061-T4 alloy by sol–gel derived micro and nano-scale hydroxyapatite (HA) Coating. J Sci Technol. 2012;12:2813–8.
14. Kim HW, Koh YH, Li LH, Lee S, Kim HE. Hydroxyapatite coating on titanium substrate with titania buffer layer processed by sol–gel method. Biomaterials. 2004;25:2533–8.
15. Montenero A, Gnappi G, Ferrari F, Cesari M, Salvioli E, Mattogno L, et al. Sol–gel derived hydroxyapatite coatings on titanium substrate. J Mater Sci. 2000;35:2791–7.
16. Hsieh MF, Perng LH, Chin TS. Hydroxyapatite coating on Ti6Al4 V alloy using a sol–gel derived precursor. Mater Chem Phys. 2002;74:245–50.
17. Billotte WG. Ceramic biomaterials. In: Bronzino JD, editor. The biomedical engineering handbook. 2nd ed. Boca Raton: CRC Press LLC; 2000.
18. Ducheyne P, Radin S, Heughebaert M, Heughebaert JC. Calcium phosphate ceramic coatings on porous titanium: effect of structure and composition on electrophoretic deposition, vacuum sintering and in vitro dissolution. Biomaterials. 1990;11:244–54.
19. Murugan R, Ramakrishna S. Development of nanocomposites for bone grafting. Compos Sci Technol. 2005;65:2385–406.
20. Bogdanoviciene I, Beganskiene A, Tonsuaadu K, Glaser J, Meyer HJ, Kareiva A. Calcium hydroxyapatite, $Ca_{10}(PO_4)_6(OH)_2$ ceramics prepared by aqueus sol–jel processing. Mater Res Bull. 2006;41:1754–62.
21. Gallardo J, Galliano P, Duran A. Bioactive and protective sol-gel coatings on metals for orthopaedic prostheses. J Sci Technol. 2001;21:65–74.
22. Guglielmi M. Sol-gel coatings on metals. J Sci Technol. 1997;8:443–9.
23. Galliano P, De Damborenea JJ, Pascual MJ, Duran A. Sol-gel coatings on 316l steel for clinical application. J Sci Technol. 1998;13:723–7.
24. Balamurugan A, Balossier G, Kannan S, Michel J, Rajeswari S. In vitro biological, chemical and electrochemical evaluation of titania reinforced hydroxyapatite sol–gel coatings on surgical grade 316L SS. Mater Sci Eng C. 2007;27:162–71.
25. De Mestral F, Drew RAL. Calcium phosphate glasses and glass-ceramics for medical applications. J of Euro Ceram Soc. 1989;5:47–53.
26. Rincon JM, Callejas P. Microstructure and microanalysis of bioglasses and glass-ceramics from the $MgO\text{-}CaO\text{-}P_2O_5\text{-}SiO_2$ system with ZrO_2. In: Bioceramics and the human body. Netherlands: Springer; 1992. pp 244–49.
27. Fathi MH, Salehi M, Mortazavi V, Mousavi SB, Parsapour A. Novel hydroxyapatite/niobium surface coating for endodontic dental implant. Surf Eng. 2006;22:353–8.